Structural Flexibility of a Helical Peptide Regulates Vibrational Energy Transport Properties

Ellen H. G. Backus,[†] **Phuong H. Nguyen,**[‡] **Virgiliu Botan,**[†] **Alessandro Moretto,**[§]
Marco Crisma,[§] **Claudio Toniolo,**[§] **Oliver Zerbe,**[†] **Gerhard Stock,**[‡] **and Peter Hamm*,**[†]

Chemische Institute, Universität Zürich, Winterthurerstr. 190, CH-8057 Zürich, Switzerland; Institut für Physikalische und Theoretische Chemie, J. W. Goethe Universität, Max-von-Laue-Str. 7, D-60438 Frankfurt, Germany; and Institute of Biomolecular Chemistry, Padova Unit, CNR, Department of Chemistry, University of Padova, Via Marzolo 1, I-35131 Padova, Italy

Received: July 21, 2008; Revised Manuscript Received: September 16, 2008

Applying ultrafast vibrational spectroscopy, we find that vibrational energy transport along a helical peptide changes from inefficient but mostly ballistic below ≈270 K into diffusive and significantly more efficient above. On the basis of molecular dynamics simulations, we attribute this change to the increasing flexibility of the helix above this temperature, similar to the glass transition in proteins. Structural flexibility enhances intramolecular vibrational energy redistribution, thereby refeeding energy into the few vibrational modes that delocalize over large parts of the structure and therefore transport energy efficiently. The paper outlines concepts how one might regulate vibrational energy transport properties in ultrafast photobiological processes, as well as in molecular electronic devices, by engineering the flexibility of their components.

I. Introduction

Heat transport is relevant not only in the macroscopic world but also on the molecular scale of biomolecules and nanostuctures. To avoid overheating, e.g., after a photochemical reaction, excess energy needs to be removed efficiently.[1] Proteins transport energy through specific pathways to function as molecular machines.[2] Furthermore, an understanding of vibrational energy transport is an important prerequisite for the development of molecular electronic devices.[3] Despite its significance, very little experimental work has been done to unravel the molecular mechanisms of vibrational energy transport in *real space* (to discriminate it from intramolecular vibrational energy redistribution which is typically studied in *energy* or *state space*). Most studies have concentrated on the vibrational energy flow from a heme group in proteins into the surrounding solvent,[4–7] which has been attributed to the transport through the propionate side chain.[8] The latter is part of the heme moiety and connects it directly to the protein surface. In systems other than proteins, energy transport phenomena have been measured, e.g., through bridged azulene–anthracene compounds,[9] small molecules in solution,[10] or model membranes.[11]

Employing time-resolved infrared (IR) spectroscopy and molecular dynamics (MD) simulations, we have recently suggested that vibrational energy transport along a peptide helix occurs in a diffusive manner with the mean distance increasing only with the square root of time, $\langle \Delta x^2 \rangle \propto t$.[12,13] From the distance dependence of the peak signal we have concluded that diffusion occurs in 1D, i.e., along the helix and not through the solvent. In contrast, the vibrational energy transport through densely packed self-assembled monolayers of long-chain hydrocarbon molecules was shown to propagate ballistically, i.e., linear in time, $\Delta x \propto t$.[14] This discrepancy raises the question
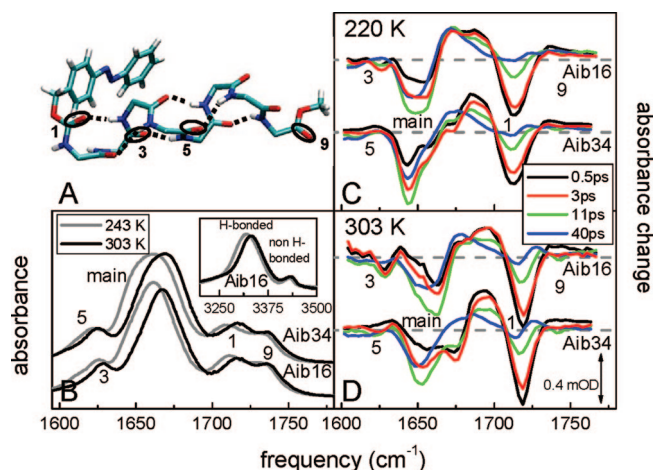
Figure 1. Molecular system and its stationary and transient pump–probe spectra. (A) X-ray diffraction structure of the peptide backbone (amino acid side chains are not shown).[12] Labels 1–9 count C=O sites with increasing distance from the azobenzene moiety. (B) FTIR absorption spectra of Aib16 and Aib34 at 243 and 323 K, respectively, in the C=O spectral region. The inset shows the NH spectrum for Aib16. (C) Transient difference spectra of Aib16 and Aib34 at 220 K at specific times after pumping the molecule in the cis configuration with a 100–150 fs pulse of 425 nm. (D) Same, but at 303 K. The data at all times are normalized to reveal identical temperature jumps by comparing the spectra at 95 ps to corresponding FTIR difference spectra.[12]

about the physical origin of these two mechanisms. Being densely packed, the latter system is probably more ordered and less flexible, which may facilitate a ballistic mechanism. In the present paper, we use temperature as a parameter to control the conformational stability of the peptide helix. We find that the structural flexibility significantly increases in a relatively narrow temperature range (260–280 K), thereby changing the mechanism of vibrational energy transport.

Our model system (Figure 1A) consist of an α-aminoisobutyric acid (Aib)-rich segment with a strong propensity to fold

* To whom correspondence should be addressed.
† Universität Zürich.
‡ J. W. Goethe Universität.
§ University of Padova.

into a 3_{10}-helix.[15] Attached to the helix is a chromophore, azobenzene, which undergoes a cis−trans isomerization after photoexcitation on a 200 fs time scale, thereby depositing a significant fraction of the pump photon energy, 3 eV, into its vibrational degrees of freedom.[12,13] To give an idea about the order of magnitude of the effect, this energy is equivalent to a local temperature of ≈1000 K (assuming that energy completely thermalizes over the vibrational degrees of freedom of the azobenzene moiety, which, of course, will not be the case on this ultrafast time scale). The impact of the isomerizing azobenzene moiety, in turn, deposits vibrational energy at the one end of the helix on the same ultrafast time scale in a highly randomized, if not thermalized, manner.[12]

The subsequent propagation of vibrational energy along the helix is monitored via C=O reporter groups, whose vibrational bands experience frequency shifts together with a broadening due to anharmonic coupling to vibrationally excited low-frequency modes.[16] As long as the anharmonic shifts are small compared to the vibrational line width of the spectator mode, one may assume that the size of the response is a linear measure of the amount of vibrational energy in the vicinity of the probe. This response averages over many low-frequency modes; hence, we cannot deduce whether energy is thermalized or not. Note that such anharmonic shifts are obtained although direct thermal excitation of the C=O reporter groups is extremely unlikely even at the high temperatures achieved in the experiment ($\hbar\omega/k_BT \ll 1$).

In order to introduce site specificity, certain amino acids (one at a time) were ^{13}C-isotope labeled to distinguish their frequency from the remainder. Since ^{13}C=O-Ala is more readily available than ^{13}C=O-Aib, we used the former, resulting in only a very little destabilization of the 3_{10}-helix.[12] Figure 1B shows IR spectra of dPAZ-Aib-^{13}C-Ala-Aib$_6$-OMe and dPAZAib$_3$-^{13}C-Ala-Aib$_4$-OMe (called Aib16 and Aib34, respectively, in the following). dPAZ (deuterated 4-phenyldiazenylbenzyloxycarbonyl) is the azobenzene moiety used for local deposition of vibrational energy. The bands at ≈1625, 1660, 1720, and 1730 cm^{-1} are assigned to the isotope labeled sites 3 or 5, the main band originating from all the nonlabeled amino acids, C=O #1 (an urethane group) and C=O #9 (an ester group), respectively. Isotope labeling red-shifts the amide I frequency by ≈35 cm^{-1} from the main band, whereas sites 1 and 9 are blue-shifted because of their different chemical environment. These spectrally isolated bands will serve as local thermometers at sites 1, 3, 5, and 9. The molecules were dissolved in chloroform (concentration ≈ 8 mM), a weakly interacting solvent of low polarity, thereby minimizing vibrational energy transport into the solvent as well as mimicking the hydrophobic environment inside a protein. Furthermore, chloroform remains a liquid in the temperature range of interest.

II. Materials and Methods

Synthesis. Deuterated PAZ-Aib-OH was synthesized by nitrating toluene-d_8 to p-nitrotoluene, oxidizing to p-nitrobenzoic acid, reducing with zinc to p-aminobenzoic acid, and then making the methyl ester using methanol and thionyl chloride. Reduction of the ester with lithium−aluminium−deuteride[17] leads to the fully deuterated p-aminobenzyl alcohol. Nitrosobenzene-d_5 was obtained by reduction of nitrobenzene-d_5 as described in ref 18. Coupling these two deuterated compounds and covalently linking the resulting alcohol to L-Ala* and Aib was performed in the same way (via PAZ-Cl) as reported in refs 19 and 20. Peptide synthesis was performed in solution by

activating the carboxyl function with 1-[3-(dimethylamino)propyl]-3-ethylcarbodiimide and 7-aza-1-hydroxy-1,2,3-benzotriazole.[21] For details of the peptide synthesis and the characterization of the molecules by IR, NMR, and X-ray diffraction, we refer to ref 12.

Time-Resolved Experiments. The peptides were investigated by UV-pump−IR-probe spectroscopy exciting *cis*-azobenzene at a wavelength of 425 nm and probing the amide I region with an IR-probe pulse centered at 1680 cm^{-1} (spectral width 200 cm^{-1}). The probe pulse was frequency dispersed in a spectrometer and imaged onto a 64-channel IR array detector covering the total region of C=O vibrations. The time resolution of the apparatus was 200 fs. The sample was dissolved in CHCl$_3$ at a concentration of typically 8 mM, circulated in a closed cycle CaF$_2$ flow cell inside a temperature-controlled N$_2$ flow cryostat with optical path length of 100 μm, and continuously irradiated with CW light at 320 nm (fwhm 70 nm) from a properly filtered Hg lamp in order to accumulate the cis species to about 80%.

Computational Methods. All simulations were performed with the GROMACS program suite,[22] using the GROMOS96 force field 43a1[23] to model the PAZ-Aib$_8$-OMe peptide and the rigid all-atom model of ref 24 to describe the chloroform solvent. Additional force field parameters for the azobenzene unit were derived from density functional theory as described in ref 25. Starting with a 3_{10}-helical conformation, the PAZ-Aib$_8$-OMe peptide was placed in an octahedral box containing ≈700 chloroform molecules. After energy minimization, the system was simulated for 40 ns at NTP conditions at temperatures 220, 250, 260, 270, 280, and 300 K. For details, see ref 12.

III. Experimental Results

Parts C and D of Figure 1 show transient UV-pump−IR-probe difference spectra of Aib16 and Aib34 for 220 and 303 K, respectively. At 303 K (Figure 1D), strong sharp bleach signals are observed already 0.5 ps after photoexcitation for site 1 in both molecules Aib16 and Aib34 as well as for site 3 in Aib16 (black spectra). The instantaneous appearance of these signals results from the impact of the photoisomerizing azobenzene moiety.[12] Subsequently, band 1 decays, while band 3 first increases, peaks at ≈3 ps, and decays afterward. Comparing parts C and D of Figure 1, it is clear that less vibrational energy reaches site 3 at lower temperatures. A comparable bleach signal is measured for site 5 (via Aib34) only after ≈3 ps at higher temperatures. The main band, as well as band 9, exhibits a growing blue shift at later times, which we attribute to a secondary effect, i.e., a slight destabilization of the hydrogen bonds due to heating of the bulk solvent.[12]
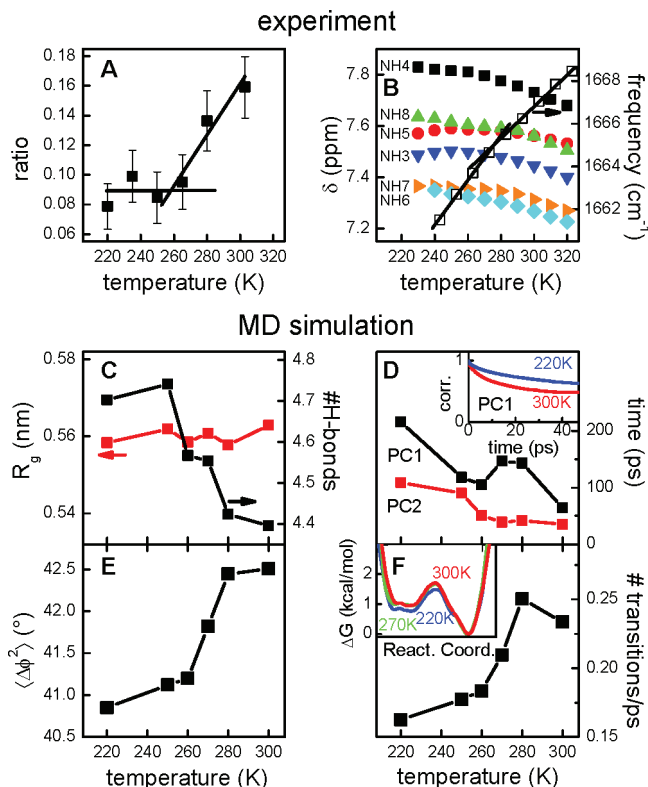
The dynamics of sites 1, 3, and 5 are summarized in Figure 2 at a series of solvent temperatures. At sufficiently long delay times, signals at all sites 1, 3, and 5 decay exponentially with a time constant of ≈7 ps. As discussed in our previous paper,[12] such a bleach−originating from anharmonic shifts due to vibrational excitation of low-frequency modes[16]−associated with a ≈7 ps decay component, known as a typical cooling time in chloroform,[26] is assigned to vibrational energy in the vicinity of the corresponding C=O group. At the larger temperature (e.g., 303 K), vibrational energy is relayed from site 1 over site 3 to site 5 with maxima that appear in a sequential order. Note that we did not observe any heat signal for site 5 in our previous report were the temperature was only a few degrees lower.[12] This is due to the lower peptide concentration in this new set of experiments, resulting in a higher heat signal relative to the interfering secondary effect of the main band (which originates from heating of the bulk solvent and hence also includes

Structural Flexibility of a Helical Peptide

J. Phys. Chem. B, Vol. 112, No. 48, 2008 **15489**
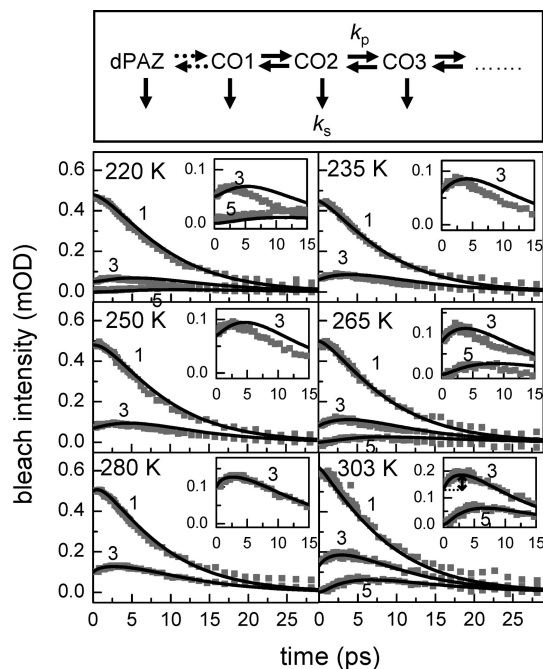
Figure 2. Energy transport: time dependence of the bleach intensity (with opposite sign as in Figure 1 and background corrected) of sites 1, 3, and 5 (symbols) at different temperatures. Bands 1 and 3 originate from Aib16 and band 5 from Aib34 (site 5 has been measured only for three temperatures). The arrow in the inset of the bottom-right panel depicts the data that enter Figure 3A. The black lines show global fits according to a master equation (see top panel, the scheme is expanded on the right) with a cooling rate (k_s) to the solvent of 1/(7 ps) for all temperatures and a propagation rate constant (k_p) varying from 1/(1.5 ps) at high temperature (303 K) to 1/(5 ps) at low temperature (220 K).

Figure 3. Comparison of experimental and MD results: (A) The heat signal increase of site 3. The error bars are to be considered an upper limit since the noise of the raw data, which enter into (A), is to some extent correlated. The lines are to guide the eye. (B) Frequency of the main band of Aib34 as a function of temperature (right axis) and chemical shifts of the H-bonded amide NH protons (left axis) of Aib34 as a function of temperature, measured at 500 MHz proton frequency. Sequential resonance assignments were based on ROESY data, and the position of Aib following Ala was confirmed by ^{13}C-decoupling. (C) Average number of helix-stabilizing hydrogen bonds (black, right axis) and radius of gyration (red, left axis), calculated from the MD simulation. (D) Decay time τ of a stretched-exponential fit $\exp(-t/\tau)^{0.5}$ to the autocorrelation function (see inset) of the first two dihedral angle principal components (PC1 and PC2). (E) Root-mean-square fluctuations of all backbone dihedral angles. (F) Number of interbasin transitions between the two dominant free energy basins shown in the inset along a linear combination of its first two principal components.

contributions from unpumped molecules). At the lower temperature (220 K), in contrast, site 5 still reveals only a very broad response (Figure 1C), the kinetics of which resembles that of site 9 or the main band (Figure 2), and we assign this signal to heating of the solvent.

At temperatures ≥280 K, the overall response can be very well fit using a simple master equation according to the scheme shown in Figure 2, top panel. In this model, each site exchanges vibrational energy with the nearest neighbors (propagation rate k_p) and at the same time cools into the solvent (cooling rate k_s). Vibrational energy is initially deposited in the dPAZ compound as well as to sites 1 to 3, mimicking the impact of the switching azobenzene moiety. After the initial deposition of vibrational energy, the helix is basically decoupled from the dPAZ unit (therefore the dotted arrow in the scheme Figure 2, top panel), although a very weak coupling is needed to explain the experimentally obtained flatness of the signal for site 1 in the first picosecond.[12] The fit of the data for 303 K (black line) reveals a cooling rate $k_s = (7\ \text{ps})^{-1}$ and a propagation rate $k_p = (1.5\ \text{ps})^{-1}$, slightly faster than the $(2\ \text{ps})^{-1}$ previously obtained at room temperature.[12] At lower temperature, vibrational energy propagation drops, e.g., at 280 K the fit gives $k_p = (3\ \text{ps})^{-1}$ while the cooling rate k_s remains essentially constant. Surprisingly, though, the diffusive model can no longer describe the data at 265 K and below (see insets in Figure 2). If the fit is forced to model the intensity of signal 3 correctly, the maximum appears too late, whereas, vice versa, adjusting the time of the maximum renders the intensity too large (the signal of site 5 is too small in this temperature range to reliably analyze its deviation from the diffusive fit). Within the framework of a diffusive model, reducing the propagation rate k_p will reduce

the amplitude at site 3, since it is in competition with cooling into the solvent k_s, but at the same time will also delay its appearance. Apparently, at low temperatures the transport is no longer diffusive. Only a relatively small fraction of the total energy is still transported at low temperatures, however, on a time scale faster than a diffusive model would predict. Since diffusion is related to slowing down a process due to scattering events, we conclude that this small fraction of energy is transported in mainly a ballistic manner.

To compare the transport efficiencies at different temperatures in a model-independent way, Figure 3A plots as a function of temperature the intensity raise of band 3 from time zero to the time when it reaches its maximum, as depicted by the arrow in Figure 2 (inset of the bottom-right panel). This signal is normalized to that at site 1, which we relate to the vibrational energy that had entered the helix, and is corrected for the decay due to cooling of the part of vibrational energy that is deposited on site 3 instantaneously due to the impact of the isomerizing azobenzene moiety. The vibrational energy transport capability is essentially constant from 220 to 265 K and rises steeply above. Clearly, with the present signal-to-noise ratio, we cannot decide

what the functional form of the temperature dependence is and to what extent the turnover is abrupt (the two lines are to guide the eyes only). This finding is nevertheless surprising for two reasons: First, the common theory of heat transport in proteins predicts a gradual, monotonic *decrease* of thermal diffusivity with temperature,[27−29] in contrast to our observation (since Figure 3A is a relative measure, it refers to the thermal *diffusivity*, and not the thermal *conductivity*; the latter would indeed increase with increasing temperature[28]). Second, the fact that not only the size (Figure 3A) but also the temporal response (Figure 2, insets) changes character around 260−280 K supports the conclusion that some sort of transition is taking place at this temperature.

The bulk solvent, chloroform, does not undergo any phase transition in the temperature range from 260 to 280 K (its melting point is 210 K). Furthermore, the intensity ratio between the two bands in the NH region (Figure 1B, inset), which is indicative for a 3_{10}-helix,[30] does not change with temperature, evidencing that the helix remains intact over the whole temperature range. These two bands originate from the intra-helical hydrogen bonded and N-terminal non-hydrogen-bonded amide protons. The small change in the slope of the vibrational frequency of the main band as a function of temperature (Figure 3B), on the other hand, indicates a change in flexibility of the helix. To further support this interpretation, we have also measured proton NMR spectra (Figure 3B): at temperatures below ≈260−280 K, only minor temperature coefficients are obtained, while they are considerably larger above, consistent with the view that the corresponding hydrogen bonds become less persistent. We also know from the NMR measurements that the molecules aggregate to a certain extent at the concentrations used, most likely in a head-to-tail manner. This effect is superimposed to the temperature dependent flexibility of the molecule and hence hampers an unambiguous interpretation of the NMR data. We have however verified through concentration-dependent measurements (ranging from 3 to 15 mM, only maximal 10% of the molecules aggregate at the lower concentration) of the effect shown in Figure 2 that the essential observation of this work, i.e. the switch of energy transport from ballistic to diffusive as a function of temperature, is not affected at all by aggregation.

It is interesting to note that a temperature shift of the amide I band with a kink, which is very similar to the one we show in Figure 3B, has been discussed in the context of the so-called glass transition of proteins.[31] Also, the shape of the curve in Figure 3A strongly resembles that of, e.g., the homogeneous line width of vibrational probes in proteins around that glass transition.[32] The glass transition is a dynamical transition occurring at ≈200 K in proteins, whose physical origin, however, is still discussed controversially.[32−41] In simple words, the molecules are trapped in various, essentially harmonic energy basins below the glass temperature T_g, whereas they are free to structurally diffuse above. Although the concept of a glass transition in the context of peptides is by far less documented in literature, it has been used, e.g., to characterize the folding properties of small peptides that do form well-defined secondary structures.[42,43]

IV. Simulation Results

To support the view of a glass transition for our model system, we performed all-atom MD simulations. Overall, we found that the structure of the helix changes only little with temperature. As an example, Figure 3C shows that the radius of gyration virtually remains constant at all temperatures, which is in

agreement with the small change of the NH FTIR spectrum in Figure 1B, inset. However, the average number of helix-stabilizing hydrogen bonds clearly drops above the transition temperature (Figure 3C), in agreement with the NMR results (Figure 3B). At the same time, the fluctuations of the backbone dihedral angles increase, as shown in Figure 3E. This plot is essentially identical to Figure 2b of ref 41—in terms of its sigmoidal shape, the size of the effect (≈5%), and the width of the transition (≈20 K)—where it has been used as a signature indicative for the glass transition in a protein, myoglobin. The smoothness of the transition also shows that the glass transition is, of course, not a true phase transition with an infinitely sharp crossover, neither in our case nor in the case of larger peptides and proteins. Rather, the highly nonlinear character of the Boltzmann factor causes a rather abrupt rise of the structural flexibility in a relatively narrow temperature range.

In addition, the MD simulations allow studying the change of dynamics at the transition temperature. In order to identify the essential dynamics of the multidimensional system in terms of the most relevant collective coordinates, we performed a principal component analysis of the backbone dihedral angles[44] and characterized the time scale of the peptide fluctuations by considering the autocorrelation functions of the first few principal components.[41] Interestingly, for all temperatures, these autocorrelation functions could be well fitted by a stretched exponential function, $\exp(-t/\tau)^\beta$, with one common stretching factor $\beta = 0.5$. Stretched exponential relaxation is frequently used as indicative for a glassy state.[36,43] Figure 3D displays the decay times τ of the first two principal components as a function of temperature. As expected, the fluctuations are faster at higher temperatures (Figure 3D) and their amplitude increases as well (Figure 3E). The relaxation time of the first principal component shows a peak at the transition temperature, whereas the remaining principal components exhibit a temperature dependence similar to the second component with a steplike drop. The small stretching factor $\beta = 0.5$ is responsible for the fact that these fluctuations have a considerable contribution on a few picoseconds time scale (Figure 3D, inset), although the overall kinetics described by τ is much slower. The amount of these fast fluctuations rises steeply above the transition temperature, in accordance with recent photon echo experiments by Fayer,[32] who observed an abrupt rise of the homogeneous dephasing rate of vibrational probes embedded in proteins (homogeneous dephasing is caused by exactly such fast fluctuations with subpicosecond correlation times).

The hallmark of a glass transition is the ruggedness of the free energy landscape in relation to temperature.[36] Below the transition temperature T_g, various conformations of the system are trapped in different energy basins, whereas thermal energy is sufficient above T_g to overcome the barriers separating these wells and conformations may therefore interchange more quickly. To understand how this effect comes about, the free energy landscape of the peptide along a linear combination of its first two principal components is depicted in Figure 3F, inset. The free energies associated with two local minima, as well as the barrier between them, changes only little with temperature, indicating that there is no large entropic contribution to the free energy. Because of the rise in thermal energy, though, the number of interbasin transitions shown in Figure 3F increases significantly when the temperature approaches $T_g \approx 270$ K. Moreover, these transitions occur on a time scale of a few picoseconds, which is also the time scale of energy transport. The temperature dependence of the interbasin transitions thus

provides a direct link between the free energy landscape and the efficiency of vibrational energy transport capabilities.

V. Discussion and Conclusions

Figure 3A unambiguously shows that vibrational energy transport increases with temperature, in contrast to common harmonic theories of heat transport in proteins[27–29] that work on the basis of a static molecule. Furthermore, a series of observations suggest a transition taking place at $\approx 260-280$ K, above which the molecule becomes more flexible, affecting both the mechanism as well as the efficiency of vibrational energy transfer. We find more or less the same transition temperature in (i) the time dependence of vibrational energy transport that is consistent with a diffusive model only above that transition temperature (Figure 2), (ii) the overall vibrational energy transport efficiency that rises steeply above that transition temperature (Figure 3A), (iii) stationary IR and NMR spectra that hint to less persistent hydrogen bonds above that transition temperature (Figure 3B), and (iv) the MD results that exhibit the signatures of a glass transition (Figure 3C–F).

These combined observations allows us to explain the results as follows. The energy initially deposited through the impact event of the isomerizing azobenzene moiety will be distributed over various normal modes of mainly site 1 in a rather randomized, unspecific manner.[12,13] The fraction of the energy contained in low-frequency modes will propagate through the helix relatively efficiently, since these low-frequency modes tend to be delocalized over large parts of the helix.[27–29,45] For a regular backbone structure, like the 3_{10}-helix, these low-frequency modes are expected to be phonon-like, and hence energy will be transported ballistically. However, this mechanism applies only for a relatively small fraction of the total energy. The majority will be contained in high-frequency modes which localize to single sites and, hence, cannot directly contribute to the transport. At low temperatures, at which the molecule is rigid on the time scale of the experiment, vibrational energy redistribution (IVR) is inefficient, and little possibility of refeeding energy from localized high-frequency modes into transporting low-frequency modes exists. As the temperature increases above the glass transition, the molecule becomes more flexible. As a result, vibrational eigenstates are constantly remixing and IVR becomes significantly more efficient, opening a channel for this refeeding. In addition, the onset of interbasin large amplitude motion with high anharmonicity further enhances IVR when approaching T_g.[29] Energy relaxation is probabilistic and energy transport now will be diffusive-like in the sense that it can be fitted by a master equation depicted in Figure 2, top panel. In agreement with our previous paper,[13] we however conclude that the rate-limiting step in energy transport is not the transport itself (which is expected to be ballistic on this short length scales[14]), but the refeeding of energy into a relatively small subset of transporting modes. Similar conclusions have been drawn for the transport through a bridged azulene–anthracene compound.[9]

Like in our model system, an energy equivalent of a visible photon is dissipated on an ultrafast subpicosecond time scale also in many photobiological processes such as the photoisomerization of retinal in rhodopsin during the process of vision[46] or the quenching of excitation energy in antenna complexes by carotenoids in the photosynthetic apparatus.[47] A similar situation is expected for newly developed molecular electronic devices or nanostructures. Such processes result in enormous temperature gradients as large as many 100 K over length scales of a few chemical bonds only. Under these extreme conditions, vibrational energy transport is no longer diffusive in the same way as known from macroscopic physics. This is since thermalization *within* an individual building block of a macromolecule is not necessarily significantly faster than thermalization *between* building blocks. Here, we have outlined a concept how one can regulate energy transport properties of molecular devices under these extreme conditions by engineering the flexibility of their components. Nature might have applied these concepts to optimize ultrafast photobiological processes, and the same might be relevant for man-made molecular electronic devices.

References and Notes

(1) Champion, P. M. *Science* **2005**, *310*, 980–982.
(2) Ota, N.; Agard, D. A. *J. Mol. Biol.* **2005**, *351*, 345–354.
(3) Chang, C. W.; Okawa, D.; Majumdar, A.; Zettl, A. *Science* **2006**, *314*, 1121–1124.
(4) Miller, R. J. D. *Annu. Rev. Phys. Chem.* **1991**, *42*, 581–614.
(5) Lian, T.; Locke, B.; Kholodenko, Y.; Hochstrasser, R. M. *J. Phys. Chem.* **1994**, *98*, 11648–11656.
(6) Li, P.; Champion, P. M. *Biophys. J.* **1994**, *66*, 430–436.
(7) Mizutani, Y.; Kitagawa, T. *Science* **1997**, *278*, 443–445.
(8) Sagnella, D. E.; Straub, J. E. *J. Phys. Chem. B* **2001**, *105*, 7057–7063.
(9) Schwarzer, D.; Kutne, P.; Schröder, C.; Troe, J. *J. Chem. Phys.* **2004**, *121*, 1754–1764.
(10) Wang, Z. H.; Pakoulev, A.; Dlott, D. D. *Science* **2002**, *296*, 2201–2203.
(11) Deàk, J. C.; Pang, Y. S.; Sechler, T. D.; Wang, Z. H.; Dlott, D. D. *Science* **2004**, *306*, 473–476.
(12) Botan, V.; Backus, E. H. G.; Pfister, R.; Moretto, A.; Crisma, M.; Toniolo, C.; Nguyen, P. H.; Stock, G.; Hamm, P. *Proc. Natl. Acad. Sci. U.S.A.* **2007**, *104*, 12749–12754.
(13) Backus, E. H. G.; Nguyen, P. H.; Botan, V.; Pfister, R.; Moretto, A.; Crisma, M.; Toniolo, C.; Stock, G.; Hamm, P. *J. Phys. Chem. B* **2008**, *112*, 9091–9099.
(14) Wang, Z.; Carter, J. A.; Lagutchev, A.; Koh, Y. K.; Seong, N.-H.; Cahill, D. G.; Dlott, D. D. *Science* **2007**, *317*, 787–790.
(15) Toniolo, C.; Benedetti, E. *Trends Biochem. Sci.* **1991**, *16*, 350–353.
(16) Hamm, P.; Ohline, S. M.; Zinth, W. *J. Chem. Phys.* **1997**, *106*, 519–529.
(17) Nystrom, R. F.; Brown, W. G. *J. Am. Chem. Soc.* **1947**, *69*, 2548–2549.
(18) Shine, H. J.; Zmuda, H.; Kwart, H.; Horgan, A. G.; Brechbiel, M. *J. Am. Chem. Soc.* **1982**, *104*, 5181–5184.
(19) Schwyzer, R.; Sieber, P.; Zatsko, K. *Helv. Chim. Acta* **1958**, *41*, 491–498.
(20) Li, C. H. *Chem. Abstr.* **1963**, *59*, 10239e–10240e.
(21) Carpino, L. A. *J. Am. Chem. Soc.* **1993**, *115*, 4397–4398.
(22) van der Spoel, D.; Lindahl, E.; Hess, B.; Groenhof, G.; Mark, A. E.; Berendsen, H. J. C. *J. Comput. Chem.* **2005**, *26*, 1701–1718.
(23) van Gunsteren, W. F.; Billeter, S. R.; Eising, A. A.; Hünenberger, P. H.; Krüger, P.; Mark, A. E.; Scott, W. R. P.; Tironi, I. G. *Biomolecular Simulation: The GROMOS96 Manual and User Guide; Vdf Hochschulverlag AG*; ETH Zürich, 1996.
(24) Tironi, I. G.; van Gunsteren, W. F. *Mol. Phys.* **1994**, *83*, 381–403.
(25) Nguyen, P. H.; Mu, Y.; Stock, G. *Proteins* **2005**, *60*, 485–494.
(26) Dahinten, T.; Baier, J.; Seilmeier, A. *Chem. Phys. Lett.* **1998**, *232*, 239–245.
(27) Yu, X.; Leitner, D. M. *J. Phys. Chem. B* **2003**, *107*, 1698–1707.
(28) Yu, X.; Leitner, D. M. *J. Chem. Phys.* **2005**, *122*, 054902.
(29) Leitner, D. *Annu. Rev. Phys. Chem.* **2008**, *59*, 233–259.
(30) Toniolo, C.; Bonora, G. M.; Barone, V.; Bavoso, A.; Benedetti, E.; Di Blasio, B.; Grimaldi, P.; Lelj, F.; Pavone, V.; Pedone, C. *Macromolecules* **1985**, *18*, 895–902.

(31) Demmel, F.; Doster, W.; Petry, W.; Schulte, A. *Eur. Biophys. J.* **1997**, *26*, 327–335.

(32) Fayer, M. D. *Annu. Rev. Phys. Chem.* **2001**, *52*, 315–356.

(33) Hartmann, H.; Parak, F.; Steigemann, W.; Petsko, G. A.; Ponzi, D. R.; Frauenfelder, H. *Proc. Natl. Acad. Sci. U.S.A.* **1982**, *79*, 4967–4971.

(34) Doster, W.; Cusack, S.; Petry, W. *Nature (London)* **1989**, *337*, 754–756.

(35) Rasmussen, B. F.; Stock, A. M.; Ringe, D.; Petsko, G. A. *Nature (London)* **1992**, *357*, 423–424.

(36) Onuchic, J. N.; Luthey-Schulten, Z.; Wolynes, P. G. *Annu. Rev. Phys. Chem.* **1997**, *48*, 545–600.

(37) Réat, V.; Dunn, R.; Ferrand, M.; Finney, J. L.; Daniel, R. M.; Smith, J. C. *Proc. Natl. Acad. Sci. U.S.A.* **2000**, *97*, 9961–9966.

(38) Lee, A. L.; Wand, A. J. *Nature (London)* **2001**, *411*, 501–504.

(39) Fenimore, P. W.; Frauenfelder, H.; McMahon, B. H.; Parak, F. G. *Proc. Natl. Acad. Sci. U.S.A.* **2002**, *99*, 16047–16051.

(40) Cornicchia, E.; Marconi, M.; Onori, G.; Paciaroni, A. *Biophys. J.* **2006**, *91*, 289–297.

(41) Moritsugu, K.; Smith, J. C. *J. Phys. Chem. B* **2006**, *110*, 5807–5816.

(42) Hansmann, U. H. E.; Okamoto, Y.; Onuchic, J. N. *Proteins* **1999**, *34*, 472–483.

(43) Hansmann, U. H. E.; Onuchic, J. N. *J. Chem. Phys.* **2001**, *115*, 1601–1606.

(44) Mu, Y. G.; Nguyen, P.; Stock, G. *Proteins* **2005**, *58*, 343–357.

(45) Segal, D.; Nitzan, A.; Hänggi, P. *J. Chem. Phys.* **2003**, *119*, 6840–6855.

(46) Kukura, P.; McCamant, D. W.; Yoon, S.; Wandschneider, D. B.; Mathies, R. A. *Science* **2005**, *310*, 1006–1009.

(47) Cerullo, G.; Polli, D.; Lanzani, G.; Silvestri, S. D.; Hashimoto, H.; Cogdell, R. J. *Science* **2002**, *298*, 2395–2398.